AIRS Deconvolution and Translation from the AIRS to CrIS IR Sounders

**** DRAFT ****

Howard E. Motteler
L. Larrabee Strow

UMBC Atmospheric Spectroscopy Lab
Joint Center for Earth Systems Technology

June 13, 2017

1 Introduction

Upwelling infrared radiation as measured by the AIRS [1] and CrIS [2, 6] sounders is a significant part of the long term climate record. We would like to treat this as a single data set and often want to compare radiances, for example in the analysis of simultaneous nadir overpasses (SNOs) for sounder calibration or validation. However the instruments have different spectral resolutions, channel response functions, and band spans. As a step in addressing this problem we consider the translation of channel radiances from AIRS to standard resolution CrIS.

In addition to AIRS to CrIS we also make regular use of an IASI to CrIS translation and have implemented and tested IASI to AIRS and CrIS to AIRS translations as well. The translations from IASI includes deapodization (a form of deconvolution) before reconvolution to the translation target, and work very well. In order of most to least accurate in comparison with calculated reference truth we have IASI to CrIS, IASI to AIRS, AIRS to CrIS, and finally CrIS to AIRS [?]. But aside from AIRS to CrIS, the methods used are conventional.

Translation from AIRS to CrIS involves more that basic resampling. AIRS is a grating spectrometer with a distinct response function for each channel determined by the focal plane geometery, while CrIS is a Michaelson interferometer with a sinc response function, after calibration and corrections.

In section 2 we show how to take advantage of our detailed knowledge of the AIRS spectral response functions (SRFs) and their overlap to deconvolve channel radiances to a resolution-enhanced intermediate representation, typically a 0.1 cm^{-1} grid, the approximate resolution of the tabulated AIRS SRFs.

This intermediate representation can then be reconvolved to an alternate instrument specification. Section 3 gives details and validation tests for the AIRS to CrIS translation, and section 4 for translation to an idealized grating model. For both cases deconvolution followed by reconvolution is shown to work significantly better than conventional interpolation. Both methods can be further improved with a statistical correcion. In section 5 we consider a purely statistical approach to such translations. Section 6 discusses applications and related and future work.

2   AIRS Deconvolution

The AIRS spectral response functions model channel response as a function of frequency and associate channels with nominal center frequencies. Each AIRS channel i has an associated spectral response function or SRF $\sigma_i(v)$ such that the channel radiance $c_i = \int \sigma_i(v) r(v) \, dv$, where r is radiance at frequency v. The center or peak of σ_i is the nominal channel frequency.

Figure 1 shows typical AIRS SRFs from the low and high ends of the band. Note the significant overlap in the wings. This can allow for a deconvolution to recover resolution beyond that of the response functions considered individually. The SRFs are not necessarily symmetrical, especially at the high end of the band. The dashed line on top of the third SRF is a fit of a generalized Gaussian, which we consider in more detail later in this section. Figure 2 shows channel spacing and resolving power for the AIRS L1c channel set [?]. The variable channel spacing and resolving power are due to the modular structure of the focal plane. Although not entirely regular—that is, not a simple function of frequency—the L1c channel set is more regular than the L1b channel set from which it is derived, and we mainly consider the L1c set here.

Suppose we have n channels and a frequency grid $\vec{v}$ of k points spanning the union of the domains of the functions σ_i. The grid step size for our applications is often 0.0025 cm^{-1}, the default resolution for upwelling radiance calculations with [4]. Let S_k be an $n \times k$ array such that $s_{i,j} = \sigma_i(v_j)/w_i$, where $w_i = \sum_j \sigma_i(v_j)$, that is where row i is $\sigma_i(v)$ tabulated at the grid $\vec{v}$ and normalized so the row sum is 1. If the channel centers are in in-
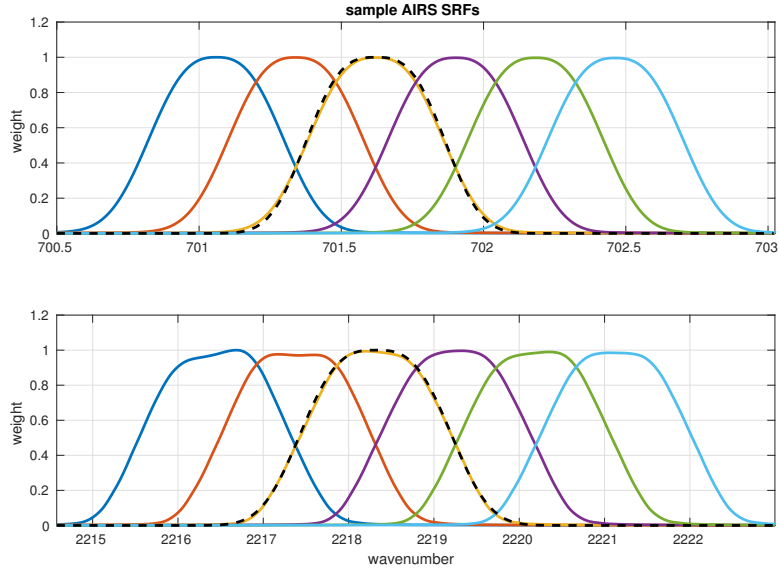
Figure 1: sample AIRS spectral response functions from the low and high ends of the band. The dashed line is a generalized Gaussian function.
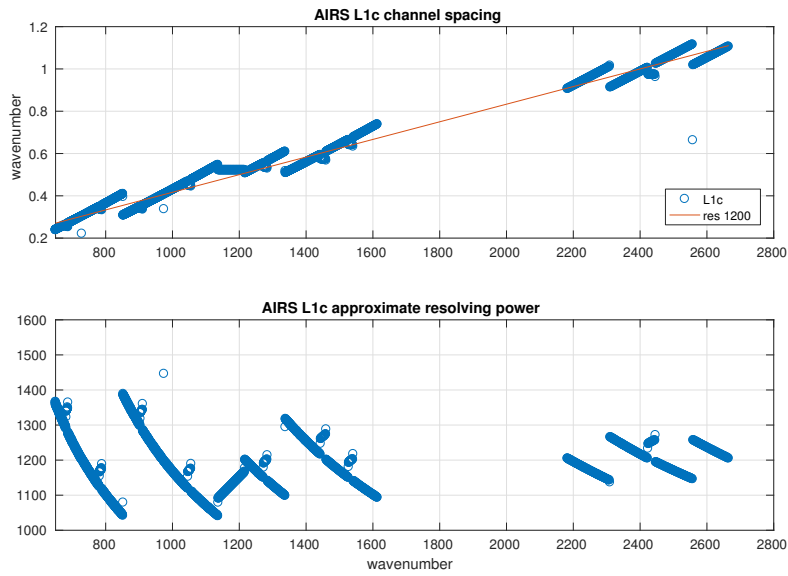

Figure 2: AIRS L1c channel spacing and derived resolving power.

3

creasing order S_k is banded, and if they are not too close (as is the case for a few of the L1b channels) the rows are linearly independent. S_k is a linear transform whose domain is radiance at the grid $\vec{v}$ and whose range is channel radiances. If r is radiance at the grid $\vec{v}$, then $c = S_k r$ gives a good approximation of the channel radiances $c_i = \int \sigma_i(v) r(v) \, dv$. In practice this is how we convolve kcarta or other high resolution calculated radiances to get AIRS channel radiances, for example for reference truth or "true AIRS" for the tests shown here.

For the AIRS to CrIS and other translations we are mainly interested in the transform S_b for SRFs at an intermediate resolution, typically 0.1 cm^{-1}. This is the approximate resolution of the SRF measurements and convenient for reconvolution to the CrIS user grid. So let $\vec{v}_b = v_1, v_2, \ldots, v_m$ be a 0.1cm^{-1} grid spanning the domains of the functions σ_i. Similar to S_k, let S_b be an $n \times m$ array where row i is $\sigma_i(v)$ tabulated at the $\vec{v}_b$ grid, with rows normalized to 1. If r is radiance at the $\vec{v}_b$ grid, then $c = S_b r$ is still a reasonable approximation of $\int \sigma_i(v) r(v) \, dv$.

For our application we want to start with c and find r, that is to deconvolve c by solving $S_b r = c$ for r. Since $m < k$, the system is underdetermined, but we can take the Moore-Penrose pseudoinverse [?] of S_b to get $r_0 = S_b^{-1} c$. This gives a minimal solution, in the sense that $||r_0||_2 \leq ||r_j||_2$ for all r_j satisfying $S_b r_j = c$. The condition number for S_b built from the L1c channels is $||S_b||_2 ||S_b^{-1}||_2 = 115$, which is tolerable.

Although our main goal is to reconvolve the 0.1 cm^{-1} intermediate representation to the CrIS or other user grids, we first compare the deconvolved radiances with reference truth from a direct convolution to intermediate grid. The choice of response functions for this direct convolution is not obvious, since the deconvolution is undoing—at least to some extent—the effects of the AIRS SRF convolutions. We chose a generalized Gaussian of the form

$$w = \exp\left(-\left(\frac{(x - v_0)^2}{2c^2}\right)^{1.5}\right)$$

where $c = \text{FWHM}/2.355$ and v_0 is the desired channel center. The exponent 1.5 was chosen to give an approximate match to AIRS SRFs with the same FWHM and channel centers, though without the fine structure and variation of the latter. Figure 1 shows two such functions paired with AIRS SRFs with the same FWHM and centers. We used this function for the 0.1 cm^{-1} intermediate grid with FWHM $= v_i/2000$ where v_i are the grid frequencies. This represents a hypothetical grating spectrometer with a resolving power of 2000, oversampled to the 0.1 cm^{-1} grid. The residual was roughly
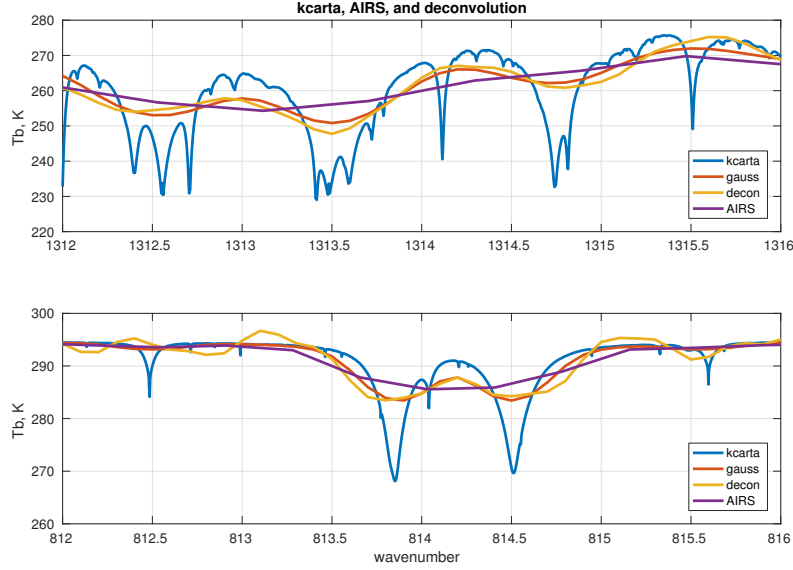
4

Figure 3: details from fitting profile 1 for kcarta, direct convolution to the 0.1 cm^{-1} grid ("gauss"), deconvolved AIRS, and true AIRS.

minimized with resolving power of 2000, as shown here. We also tried the generalized Gaussian with a fixed FWHM for values 0.4, 0.6, and 0.8 and a sinc basis with a spacing of 0.2 cm^{-1}, all of which gave larger residuals.

The AIRS deconvolution gives a modest resolution enhancement, at the cost of added artifacts and noise. Figure 3 shows details of kcarta, direct convolution to the 0.1 cm^{-1} grid ("gauss"), deconvolution, and AIRS spectra for fitting profile 1 [3, 5]. In the first subplot we see the deconvolution is capturing some of the fine structure in the kcarta data that is present in the direct convolution but not in the AIRS data. In the second subplot we see the deconvolution (and direct convolution) resolving a pair of close lines that are not resolved at the AIRS L1c resolution. But we also see some ringing that is not present in the direct convolution. Figure 4 shows the full spectra from fitting profile 1, along with sample details from the low and high ends of the band, for the deconvolution and direct convolution to the intermediate grid. In the details we see some overshoot and ringing in the deconvolution. But as noted we do not propose using the deconvolved radiances directly, they are an intermediate step in reconvolution to a lower resolution.

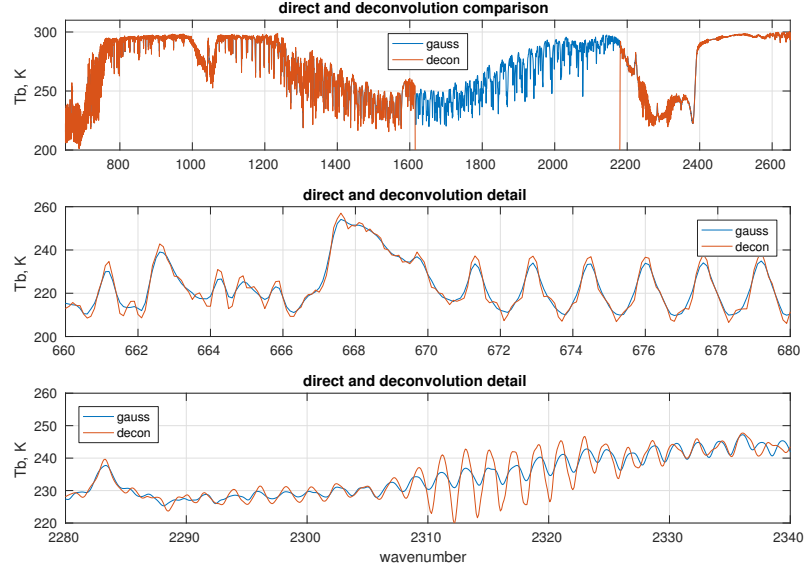Figure 5 shows a pair of typical adjacent rows of the deconvolution matrix

Figure 4: spectra from fitting profile 1 for direct convolution to the 0.1 cm^{-1} grid ("gauss") and deconvolved AIRS
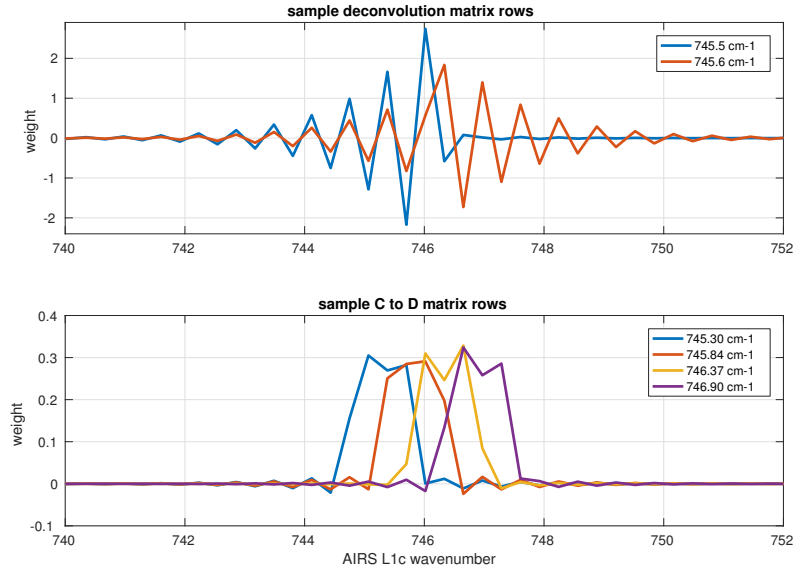

Figure 5: sample adjacent rows for the deconvolution and L1c to L1d transforms

S_b^{-1} in the first subplot. Row i of S_b^{-1} is the weights applied to L1c channel radiances to synthesize the deconvolved radiance r_i at the intermediate grid frequency v_i. The oscillation shows we are taking the closest AIRS channel, subtracting weighted values for channels ± 1 step away, adding weighted values for channels ± 2 steps away, and so on, with the weights decreasing quickly as we move away from v_i, with eight to ten L1c channels making a significant contribution to each deconvolution grid point.

The second subplot shows four adjacent rows of the matrix $S_d \cdot S_b^{-1}$, which takes L1c to L1d channel radiances. (The L1d radiances are discussed in a later section; here they are of interest mainly as a typical reconvolution.) Both matrices are banded but the bands are narrower in the second, with three to five L1c channels contributing significantly to each L1d channel. The range of influence is significant since for example we may want to see which L1d channels are derived in part from the subset of synthetic L1c channels.

3   AIRS to CrIS translation

[need intro sentence]

Given AIRS deconvolution to the 0.1 cm^{-1} intermediate grid, reconvolution to the CrIS user grid is straightforward. For the CrIS standard resolution mode the channel spacing is 0.625 cm^{-1} for the LW, 1.25 cm^{-1} for the MW, and 2.5 cm^{-1} for the SW bands. For each CrIS band, we (1) find the AIRS and CrIS band intersection, (2) apply a bandpass filter to the deconvolved AIRS radiances restricting them to the intersection, with a rolloff outside the intersection, and (3) reconvolve the filtered spectra to the CrIS user grid with a zero-filled double Fourier transform.

Translations are tested by comparison with calculated reference truth. We start with a set of atmospheric profiles and calculate upwelling radiance at a 0.0025 cm^{-1} grid with kcarta [4] over a band spanning the domains of the AIRS and CrIS response functions. "True AIRS" is calculated by convolving the kcarta radiances with AIRS SRFs and "true CrIS" by convolving kcarta radiances to a sinc basis at the CrIS user-grid. True AIRS is then translated to CrIS to get "AIRS CrIS", and this is compared with true CrIS. Figure 6 shows sample spectra for true AIRS, deconvolved AIRS, true CrIS and AIRS CrIS. The difference between true CrIS and AIRS CrIS is hard to see at this level of detail, and for the remainder of this paper we will mainly be looking at differences.

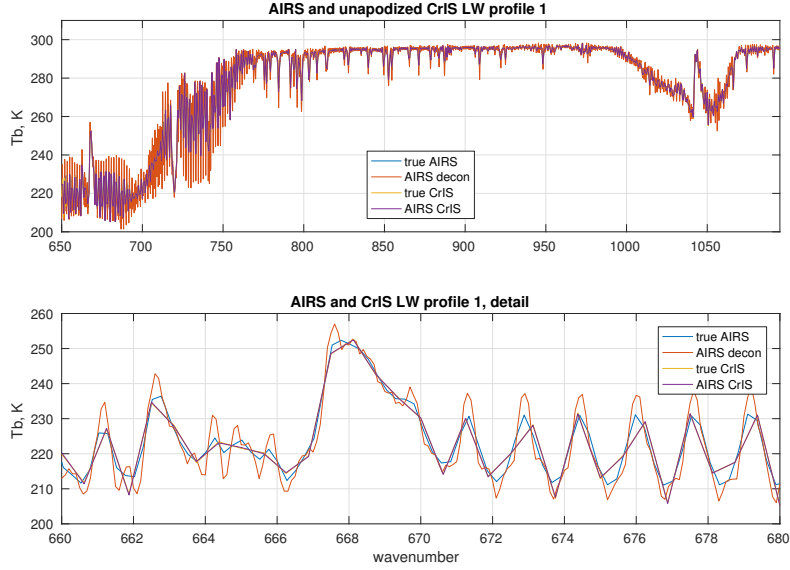For most tests we use a set of 49 fitting profiles spanning a wide range

Figure 6: true AIRS, deconvolved AIRS, true CrIS, and AIRS CrIS

of clear atmospheric conditions, initially chosen for testing radiative transfer codes [3, 5]. The set is largely uncorrelated, in the sense that reducing the reconstruction residual to 0.02 K for requires 48 left-singular vectors. (Details of this correlation measure are givein in the appendix.) For statistical correction and direct regression (discussed later) we also use a set of 7377 radiances calculated from mostly cloudy AIRS profiles spanning several consecutive days, as the dependent set. This set is moderately correlated; reducing the reconstruction residual to 0.02 K requires 260 left-singular vectors. For all cases considered here the 49 profile set gives a stricter test than splitting the 7377 profile set into dependent and independent sets as residuals with the 49-profile set are consistently larger.

Figures 7, 8, and 9 show the mean and standard deviation of true CrIS minus AIRS CrIS for the 49 fitting profiles, with and without Hamming apodization, for each of the CrIS bands. Figure 10 summarizes these results for Hamming apodized radiances. The residual has a high frequency component with a period of 2 channel steps that is significantly reduced by the apodization. The constant or DC bias (the mean of the residuals over frequency) is very close to zero for the apodized residuals.

There is some regularity in the residual, including an oscillation with period two channel steps. Up to this point there is no statistical component
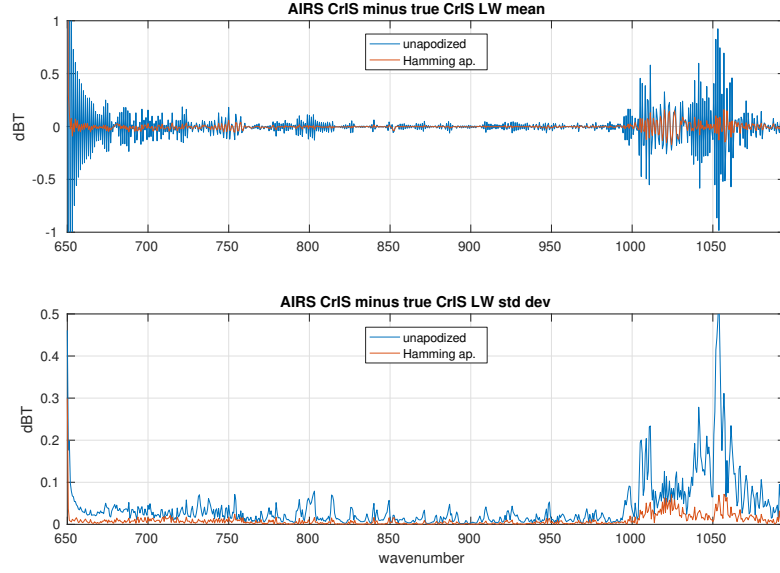
Figure 7: Mean and standard deviation of unapodized and Hamming apodized AIRS CrIS minus true CrIS, for the CrIS LW band
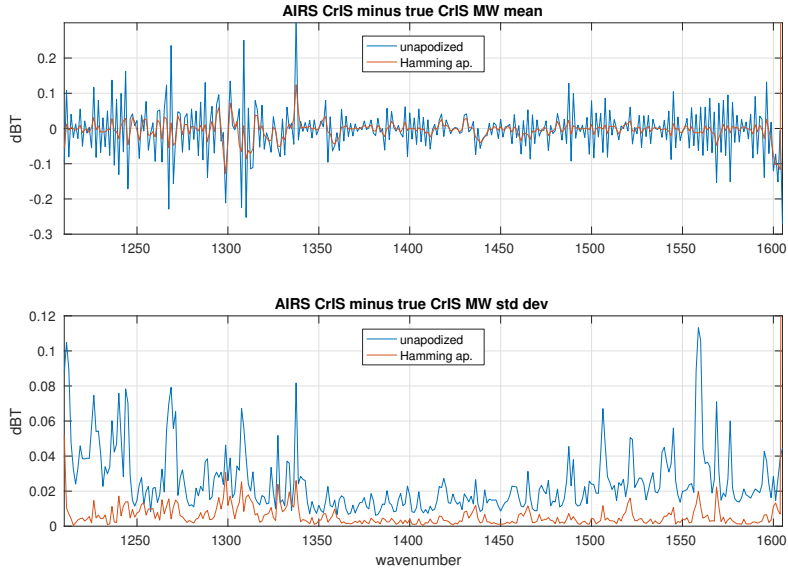

Figure 8: Mean and standard deviation of unapodized and Hamming apodized AIRS CrIS minus true CrIS, for the CrIS MW band
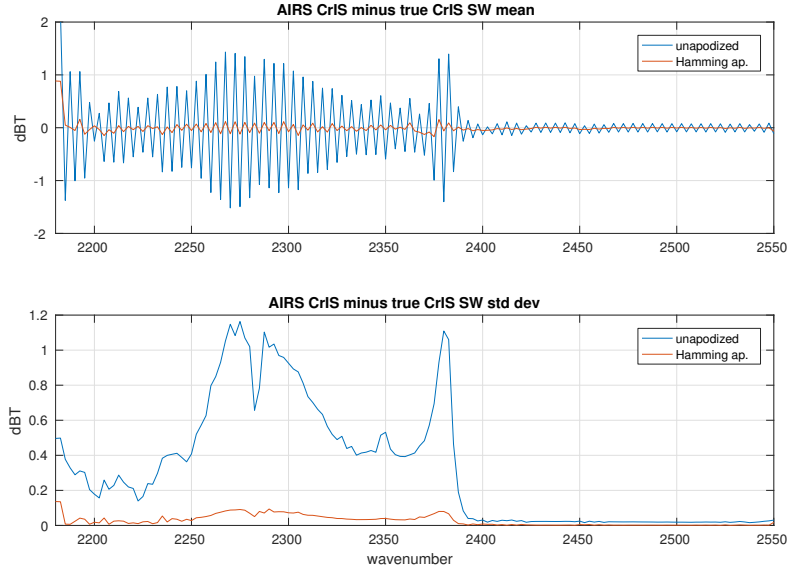
9

Figure 9: Mean and standard deviation of unapodized and Hamming apodized AIRS CrIS minus true CrIS, for the CrIS SW band
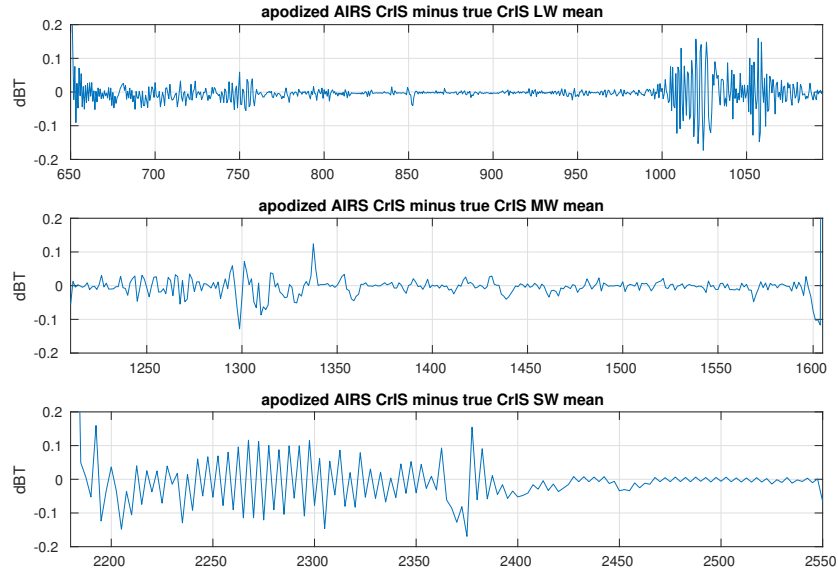

Figure 10: Mean of apodized residuals for all three CrIS bands

to our translation, beyond finding a good test set for validation. We feel it is important to be clear about any steps that require statistical fitting. That said, a simple linear correction can give a significantly further reduction in the validation residual. For the statistical tests we use the set of 7377 mostly cloudy AIRS profiles as the dependent set and the 49 profile set the independent or test set.

We compare three such corrections. These are done with a separate regression for each CrIS channel, and so introduce no cross-correlations. Let t_i^{TC} be true CrIS and t_i^{AC} AIRS to CrIS brightness temperatures for CrIS channel i, both from the dependent set. For the bias test we subtract the mean residual from the dependent set. For the linear test we find a_i and b_i to minimize $||a_i\, t_i^{\text{AC}} + b_i - t_i^{\text{TC}}||_2$ and for the quadratic test weights c_i, a_i and b_i to minimize $||c_i\, (t_i^{\text{AC}})^2 + a_i\, t_i^{\text{AC}} + b_i - t_i^{\text{TC}}||_2$.

Figure 11 is a comparison of bias, linear, and quadratic corrections for the LW band. The linear and quadratic corrections are nearly identical, and the quadratic coefficient is very close to zero. Figure 12 shows the weights for the linear fits from figure 11. The a weight is very close to 1 and the b weight to the bias. Figures 13 and 14 show the linear correction giving a similar improvement in the MW and a small improvement in the SW, where the quadratic correction is noticably worse. Figure 15 summarized results for the linear correction, pairing these with the apodized uncorrected residuals.

We can give a reasonable estimate of noise equivalent differential radiance (NEdN) as follows. We start with AIRS L1c and CrIS NEdN estimates. The L1c spec is the average over a day (4 Dec 2016) of NEdN values from the L1c granules, with gaps for the synthetic channels filled in by interpolation. The CrIS values are from a single CCAST ?? granule. The CrIS values are quite stable over time and consistent with other CrIS NEdN estimates. Results are summarized in figure 16.

Noise with a normal distribution at the AIRS spec is added to true AIRS and then measured. The measured AIRS noise is the "test" line in the plot. This is very close to the spec and so serves as a sanity check for our methods. True AIRS with added noise is then translated to CrIS and the noise of the translation is measured. This is the AIRS to CrIS line in the plots. The unapodized translation tracks the AIRS noise spec fairly closely in the LW and MW, and is a little less in the SW. Unapodized AIRS to CrIS noise is a little higher than true CrIS noise in the LW, a little less in the MW, and significantly less in the SW, and this relationship is unchanged with apodization.

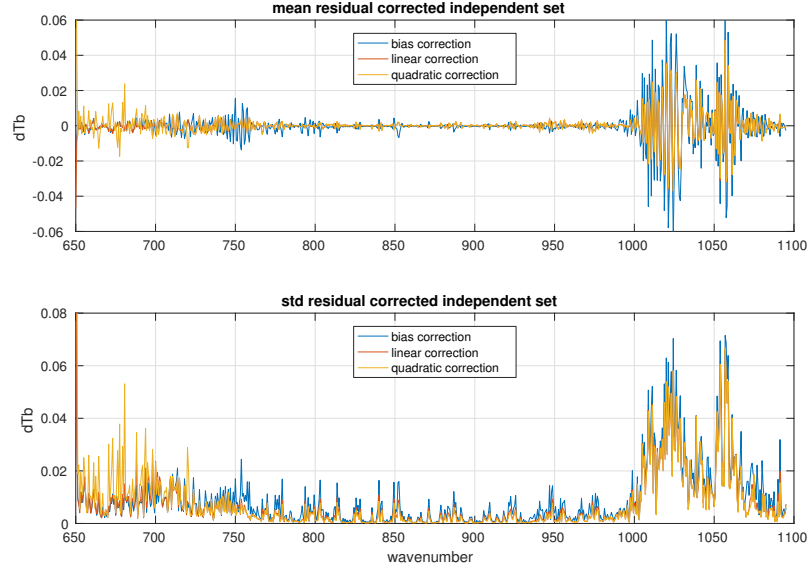Translation with deconvolution works significantly better than interpo-

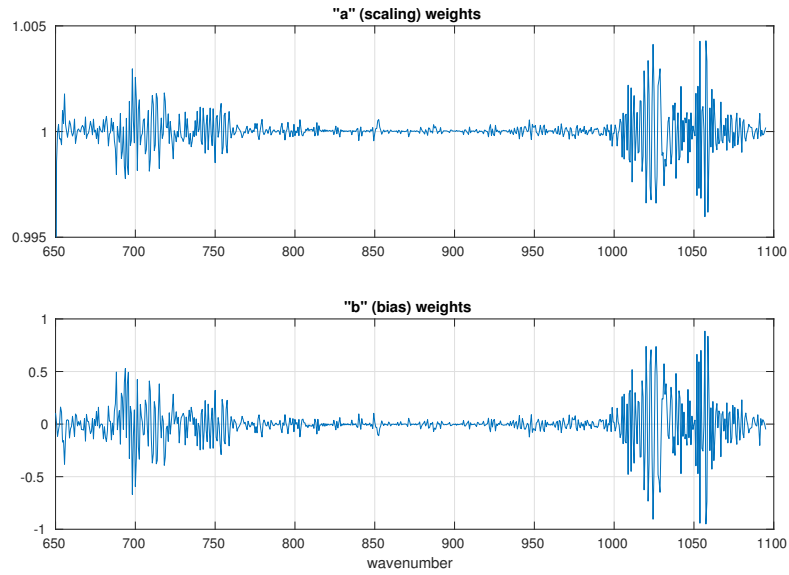Figure 11: Mean and standard deviation of LW corrected apodized residuals

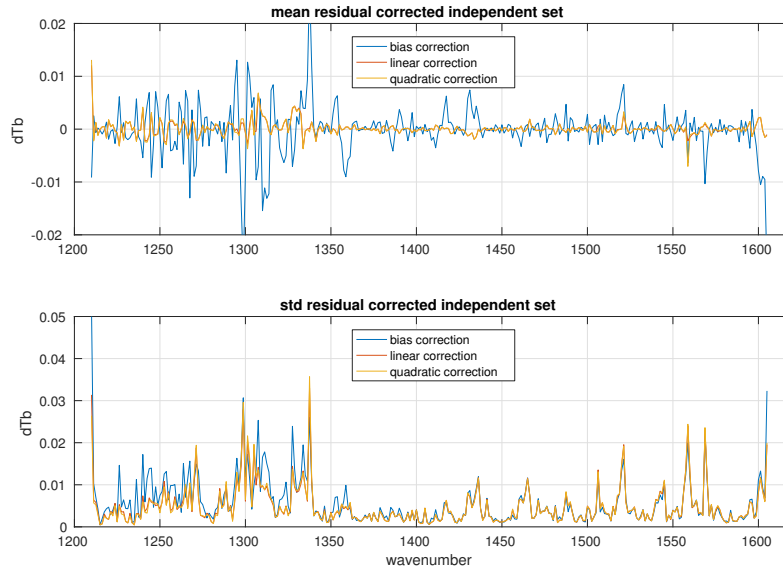Figure 12: LW a and b weights for the linear correction $ax + b$

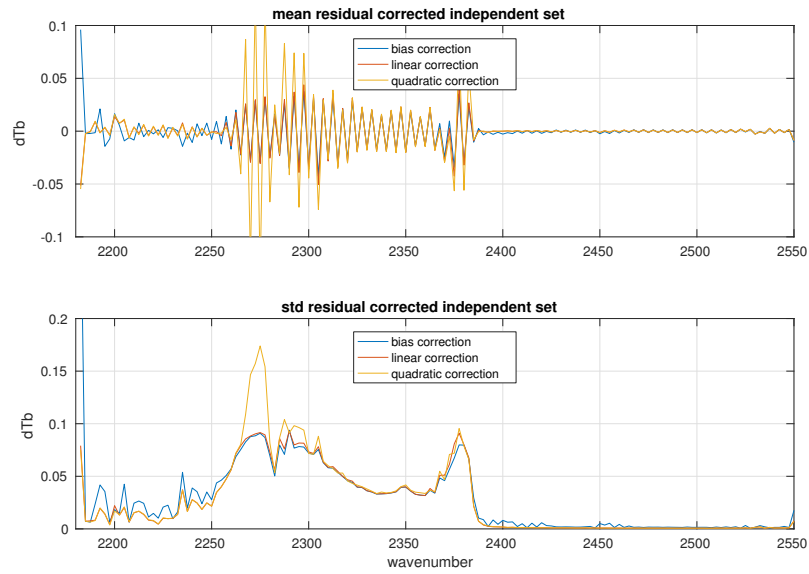Figure 13: Mean and standard deviation of MW corrected apodized residuals.

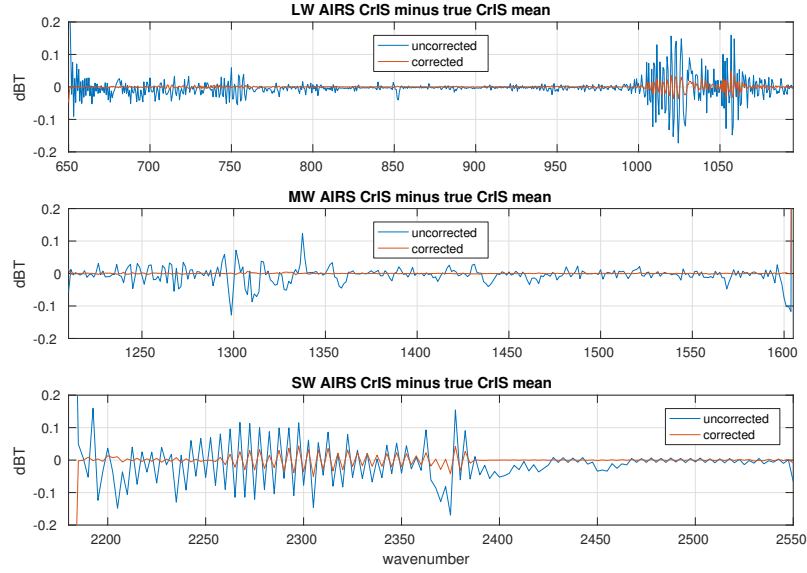Figure 14: Mean and standard deviation of SW corrected apodized residuals.

13

Figure 15: Mean corrected apodized residuals for all three bands.
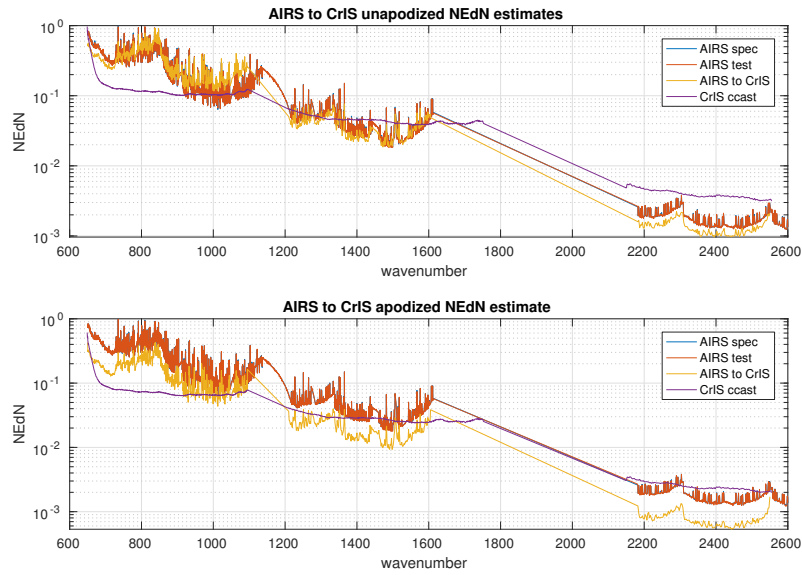

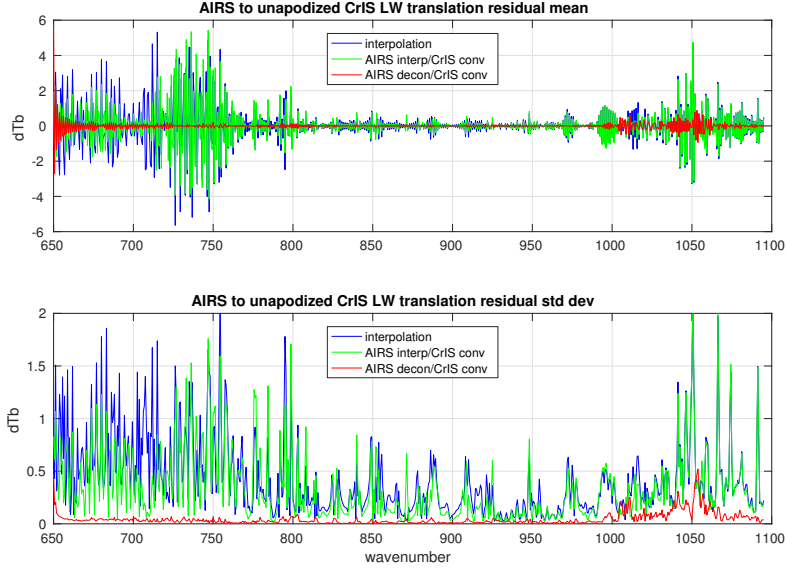Figure 16: AIRS to CrIS unapodized and apodized NEdN estimates

14

Figure 17: spline interpolation, interpolation with convolution, and deconvolution with convolution for the CrIS LW band

lation for the AIRS to CrIS translation. We consider two cases. For the first, start with true AIRS and interpolate radiances directly to the CrIS user grid with a cubic spline. For the second, interpolate true AIRS to the 0.1 cm^{-1} intermediate grid with a cubic spline and then convolve this to the use CrIS user grid. Figure 17 shows interpolated CrIS minus true CrIS for the LW band, without apodization. The two-step interpolation works a little better than the simple spline, but both residuals are significantly larger than for the translation with deconvolution. Results for the MW are similar, while the unapodized comparison is less clear for the SW. With Hamming apodization, the residuals with deconvolution are significantly less than interpolation for all three bands.

4 Translation to an idealized grating model

The AIRS deconvolution can be used for other translations. In this section we briefly consider reconvolution to idealized grating models with resolving power of 1200 and 700. Define an AIRS L1d basis with the generalized Gaussian response function above, with FWHM $= v$/resolving power and $dv = $ FWHM/2, and with the dv-spaced channel steps starting at v_0. In

contrast with the regular spacing used for the 0.1 cm^{-1} intermediate grid, this is not oversampled.

As for tests of the AIRS to CrIS translation, 'true L1c" is calculated by convolving the kcarta radiances with AIRS L1c SRFs and "true L1D" by convolving to an L1d basis with the desired resolving power and first channel frequency. L1c is translated to L1d by deconvolution followed by reconvolution to the desired L1d basis to get "L1C to D", and this is compared with true L1d.

Figure 18 shows residuals for reconvolution to an L1d basis with resolving power of 1200, the nominal AIRS resolution and figure 19 shows residuals for a resolving power of 700. Note the different x-axes for the two figures. Some resolving power is sacrificed in shifting channel centers to a single regular function of frequency. The L1d residuals dependend in part on the starting channel, and so on how the SRF peaks line up with the L1c set. The residuals above are the result of a rough fit for v_0. For a resolving power of 1200 this gave v_0 equal to the first L1c channel, while for 700 it was the first L1c channel plus 0.2 cm^{-1}.

Although some resolving power is lost in the L1c to L1d translation, the residuals for a resolving power of 1200 are roughly comparable to un-apodized CrIS, and residuals for a resolving power of 700 to apodized CrIS. As with the AIRS to CrIS translation, residuals are reduced significantly with a linear correction. Residuals for L1d with a resolving power of 700 after correction are roughly comparable to residuals for apodized CrIS after a similar correction.

As with the AIRS to CrIS translation, deconvolution is significantly better than interpolation for the L1c to L1d translation. We consider two cases. For the first, start with true L1c and interpolate radiances directly to the L1d grid with a cubic spline. For the second, interpolate true L1c to the 0.1 cm^{-1} intermediate grid with a cubic spline and convolve this to the L1d channel set. Figure 20 shows interpolated L1d minus true L1d. The two-step interpolation works a little better than the simple spline, but is still much larger than the residual for translation with deconvolution.

The L1c to L1d translation can be represented as a single linear transform $S_d \cdot S_c^{-1}$, where S_c and S_d are the transforms taking the intermediate grid to L1c and L1d channels and S_c^{-1} the pseudo-inverse of S_c, that is, the deconvolution transform. We can get such a tranform in other ways, for example by regression to find X that minimizes the residual $\|Xr_c - r_d\|_2$ for L1c and L1d radiance sets r_c and r_d. If r_c and r_d are m and n by k matrices, then if $k <= m$ we can simply solve for X. If $k < m$ the system is underdetermined; in this case the residual is zero but extrapolation behavior
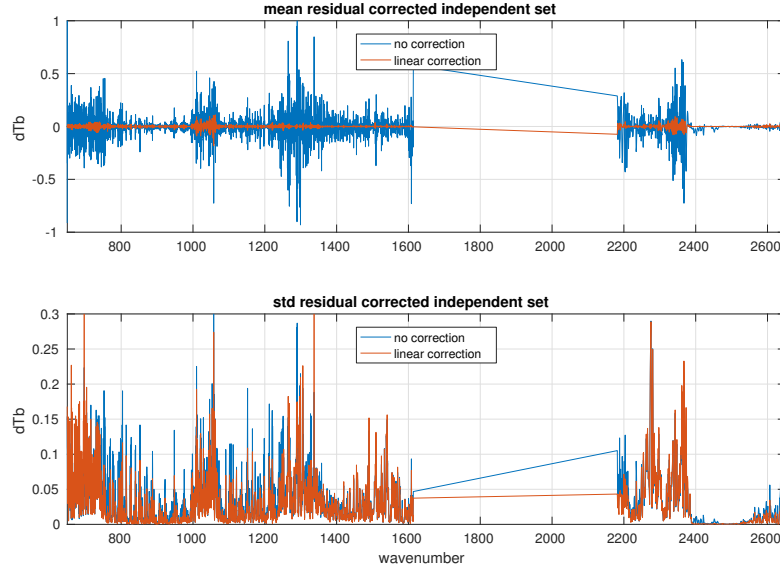
Figure 18: mean and standard deviation over the 49 fitting profiles for the
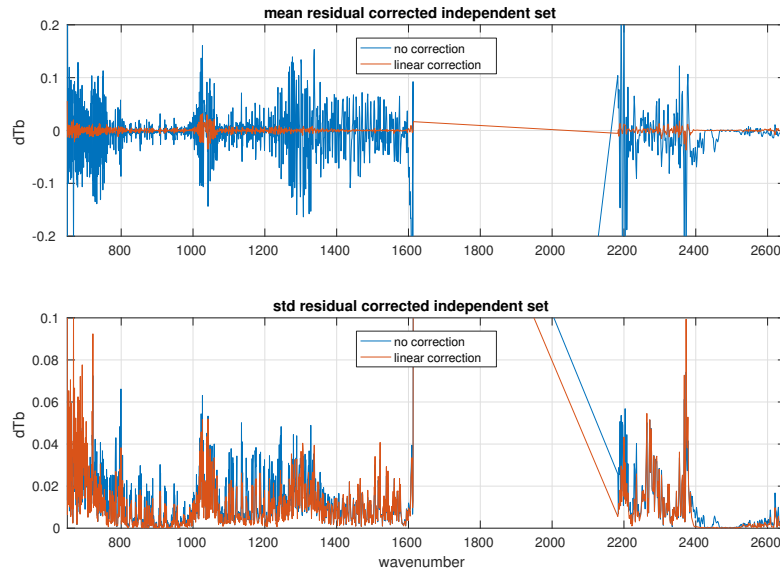L1c to L1d translation minus true L1d for a resolving power of 1200

Figure 19: mean and standard deviation over the 49 fitting profiles for the
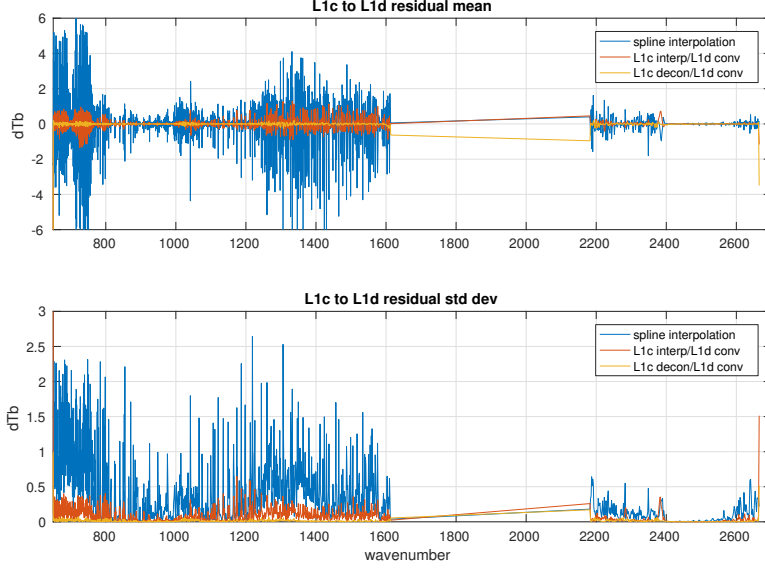L1c to L1d translation minus true L1d for a resolving power of 700

17

Figure 20: spline interpolation, interpolation with convolution, and deconvolution with convolution for the AIRS L1c to L1d translation with $v_0 = 649.822$ cm^{-1} and a resolving power of 700

is typically poor. If $k > m$ we can find X by regression, and extrapolation behavior can be quite good if we regress against large sets of representative data. In practice this seems to work very well, at least for minimizing both dependent and independent set residuals. But in contrast with the sharply banded composite transform $S_d \cdot S_c^{-1}$ the resulting transform is full of unexpected correlations and so may not be suitable for applications where we want to trace channel dependencies in the translation.

5 Direct regression

The corrections of section 3 and 4 are applied independently to each channel, while in section 5 we do the translation, including channel shifts, with a single larger regression.

The L1c to L1d translation can be represented as a single linear transform $S_d \cdot S_c^{-1}$, where S_c and S_d are the transforms taking the intermediate grid to L1c and L1d channels and S_c^{-1} the pseudo-inverse of S_c, that is, the deconvolution transform. We can get such a tranform in other ways, for example by regression to find X that minimizes the residual $\|Xr_c - r_d\|_2$

18

for L1c and L1d radiance sets r_c and r_d. If r_c and r_d are m and n by k matrices, then if $k <= m$ we can simply solve for X. If $k < m$ the system is underdetermined; in this case the residual is zero but extrapolation behavior is typically poor. If $k > m$ we can find X by regression, and extrapolation behavior can be quite good if we regress against large sets of representative data. In practice this seems to work very well, at least for minimizing both dependent and independent set residuals. But in contrast with the sharply banded composite transform $S_d \cdot S_c^{-1}$ the resulting transform is full of unexpected correlations and so may not be suitable for applications where we want to trace channel dependencies in the translation.

6 Applications and conclusions

[some notes on SNOs from SNO paper]

7 Appendix

We can use the basis size needed to get a reconstruction residual below some fixed threshold as a measure the correlation of a set of radiances. Let R be an m by n array of radiances with one row per channel and one column per observation. Let $R = U S V^T$ be a singular value decomposition with the singular values in descending order, and U_k the first k columns of U. We can simply take the singular values as one measure of correlation; these drop off more quickly for more correlated data.

For our applications a more useful measure is the number of basis vectors needed for a particular reconstruction residual. We can approximate R with a linear combination of the orthonormal vectors U_k, as $R \approx U_k U_k^T R$. The approximation improves as k increases and becomes exact for some $k <= m$. This is useful as a form of compression when k is small relative to n. For that case we save U_k and $U_k^T R$ separately. Examples of this include IASI radiance data and the kcarta absorption database.

We can think of k as a reconstruction score and for example find the smallest k such that $\mathrm{RMS}(B^{-1}(R) - B^{-1}(U_k U_k^T R)) < 0.02$ degrees K, where B^{-1} is the inverse Planck function. In this case k is the number of linearly independent vectors needed to represent the radiance data to some particular accuracy, and so a measure of the correlation of the data. For the 49 profile fitting set and a residual limit of 0.02 K, we found $k = 48$, which we would interpret as largely uncorrelated while for the 7377 profile cloudy set we found $k = 260$, which we would interpret as moderately correlated.

References

[1] H. H. Aumann, M. T. Chahine, C. Gautier, M. D. Goldberg, E. Kalnay, L. M. McMillin, H. Revercomb, P. W. Rosenkranz, W. L. Smith, D. H. Staelin, L. L. Strow, and J. Susskind. AIRS/AMSU/HSB on the aqua mission: design, science objectives, data products, and processing systems. *IEEE Transactions on Geoscience and Remote Sensing*, 41:253–264, Feb. 2003.

[2] Y. Han, H. Revercomb, M. Cromp, D. Gu, D. Johnson, D. Mooney, D. Scott, L. Strow, G. Bingham, L. Borg, Y. Chen, D. DeSlover, M. Esplin, D. Hagan, X. Jin, R. Knuteson, H. Motteler, J. Predina, L. Suwinski, J. Taylor, D. Tobin, D. Tremblay, C. Wang, L. Wang, L. Wang, and V. Zavyalov. Suomi NPP CrIS measurements, sensor data record algorithm, calibration and validation activities, and record data quality. *Journal of Geophysical Research (Atmospheres)*, 118:12734, Nov. 2013.

[3] L. Strow, S. Hannon, S. De Souza-Machado, H. Motteler, and D. Tobin. An overview of the airs radiative transfer model. *Geoscience and Remote Sensing, IEEE Transactions on*, 41(2):303–313, Feb 2003.

[4] L. Strow, H. E. Motteler, R. G. Benson, S. E. Hannon, and S. D. Souza-Machado. Fast computation of monochromatic infrared atmospheric transmittances using compressed look-up tables. *Journal of Quantitative Spectroscopy and Radiative Transfer*, 59(35):481 – 493, 1998. Atmospheric Spectroscopy Applications 96.

[5] L. L. Strow, S. E. Hannon, S. De-Souza Machado, H. E. Motteler, and D. C. Tobin. Validation of the atmospheric infrared sounder radiative transfer algorithm. *Journal of Geophysical Research: Atmospheres*, 111(D9), 2006. D09S06.

[6] L. L. Strow, H. Motteler, D. Tobin, H. Revercomb, S. Hannon, H. Buijs, J. Predina, L. Suwinski, and R. Glumb. Spectral calibration and validation of the Cross-track Infrared Sounder on the Suomi NPP satellite. *Journal of Geophysical Research (Atmospheres)*, 118:12486, Nov. 2013.